Delft University of Technology

Enhancing re-detection efficacy of defects on blank wafers using stealth fiducial markers

Bouwens, MAJ; Maas, D; van der Donck, JCJ; Alkemade, PFA; van der Walle, P

DOI
10.1016/j.mee.2016.01.007

Publication date
2016

Document Version
Accepted author manuscript

Published in
Microelectronic Engineering

Citation (APA)
Bouwens, MAJ., Maas, D., van der Donck, JCJ., Alkemade, PFA., & van der Walle, P. (2016). Enhancing re-detection efficacy of defects on blank wafers using stealth fiducial markers. *Microelectronic Engineering*, *153*, 48-54. https://doi.org/10.1016/j.mee.2016.01.007

Important note
To cite this publication, please use the final published version (if applicable).
Please check the document version above.

Copyright
Other than for strictly personal use, it is not permitted to download, forward or distribute the text or part of it, without the consent of the author(s) and/or copyright holder(s), unless the work is under an open content license such as Creative Commons.

Takedown policy
Please contact us and provide details if you believe this document breaches copyrights.
We will remove access to the work immediately and investigate your claim.

This work is downloaded from Delft University of Technology.
For technical reasons the number of authors shown on this cover page is limited to a maximum of 10.

Enhancing re-detection efficacy of defects on blank wafers using stealth fiducial markers

M.A.J. Bouwens [a,b], D.J. Maas [a], J.C.J. van der Donck [a], P.F.A. Alkemade [b], P. van der Walle [a]

[a] TNO, P.O. Box 155, 2600 AD, Delft, The Netherlands

[b] Kavli Institute of Nanoscience, Delft University of Technology, Lorentzweg 1, 2628 CJ Delft, The Netherlands

e-mail: peter.vanderwalle@tno.nl

Keywords: defect (re-)detection, particle inspection, fiducial marker, dark field microscopy, defect review, semiconductor manufacturing

Microelectronic Engineering **153** (2016) 48–54

Abstract

To qualify tools of semiconductor manufacturing, particles unintentionally deposited in these tools are characterized using blank wafers. With fast optical inspection tools one can quickly localize these particle defects. An example is TNO's Rapid Nano, which operates in optical dark field. The next step is defect review for further defect characterization. When the blank wafers are transferred to another tool, e.g. a SEM or an AFM the absolute defect position information is lost. Therefore, the re-detection of the defects in the review tool is time consuming. To enhance the re-detection speed, a fiducial marker system can be used that couples the coordinates of the fast inspection tool to the coordinates of the characterization tool.

In this work such a fiducial marker system was designed and validated. The influence of the height and the composition of the fiducial markers on the performance of the marker system was investigated using finite element analysis (by COMSOL) and experiments. The optimized fiducial markers are very visible in optical bright field and in SEM, while almost invisible ("stealth") in optical dark field. These properties make the markers both easily visible and accurately localizable in the characterization tools. The stealth fiducial marker system was fabricated and validated by re-detecting programmed test defects on a blank wafer. The experimental results are compared to a Monte Carlo simulation that takes into account the uncertainties in the coordinate transformation and localization of the test defects.

Our results show that a fiducial marker system greatly enhances the re-detection efficacy of defects on blank wafers. Using the fiducial marker system, 100% of the test defects were re-detected in SEM and AFM. A single 7x7 μm^2 SEM image suffices to meet the ITRS requirement for particles as small as 70 nm in diameter.

1. Introduction

Following Moore's law, chips in e.g. mobile phones and personal computers have shrunk and will continue to shrink [1]. As the years progress, chips become smaller, faster and more powerful. Today, state-of-the-art chips have a critical dimension of 14 nm [2] and on such a scale, a very small particle can already lead to a malfunctioning chip [3], for example by shorting a circuit or by disrupting a protective barrier layer. In fact, particle defects on lithography masks and wafers are among the main contributors to yield loss in semiconductor manufacturing [4]. Despite major efforts and successes in mitigation, contamination during manufacturing still occurs. Therefore, particle defects still need to be characterized to locate the source of the contamination, such that future particle defects can be avoided. Characteristics of interest are e.g. size, shape, and chemical composition of the particle. Manufacturing tools and processes are often qualified on particle cleanliness using blank substrates (masks or wafers, known as "blanks") as witness samples [5]. The blank passes through the tool or process of interest once or multiple times to collect particle defects. Because tools are already very clean and tool time is expensive, the defect density on the blank will be low. Hence, finding particles for characterization is very difficult [6,7]. Therefore, fast optical inspection systems are in use, capable of inspecting large areas in a reasonably short time. TNO has developed an optical inspection system, the RapidNano3, which can detect particles as small as 42 nm on substrates up to 150 mm in diameter [8]. Its basic detection principle is the strong scattering of light by particles on a flat surface.

Optical inspection tools like the Rapid Nano detect defects, but offer no information on the defect shape or composition. To characterize and classify a defect, further analysis at a higher spatial resolution is needed. The defects can be classified according to their characteristics as measured by e.g. scanning electron microscopy (SEM) [3,6] or atomic force microscopy (AFM) [7,9]. However, the latter tools, often named 'review tools', are much slower and have a small field of view. More importantly, they require the blank to be transferred, hence losing the absolute position information of the defects. Loss of position information and the small field of view mean that re-detection of the defects in the characterization tool is not trivial; for the smallest defects, a re-detection success rate of 50% is nowadays considered challenging [4]. An accurate translation of the map of all defects from the optical inspection tool to the stage coordinate system of the characterization review tool is needed to meet this challenge. One line of action to meet this challenge is a combination of a marker system and alignment sensors in the inspection and characterization tools. This is a costly and inflexible solution as each tool must have a calibrated sensor. If additional characterization is needed, one cannot move on to tools without a sensor.

Here we describe the design, development, and validation of a fiducial marker system on blank wafers that can be localized using the normal detection mechanism of the tool; in particular, by optical dark field (for fast optical inspection, e.g. in the Rapid Nano), by electron scattering (in an SEM), and optical bright field (for navigation in an AFM). By using the normal detection or navigation mechanism of a tool, no additional alignment sensor is required. The fiducial marker system enhances the re-detection rate by SEM or AFM of previously optically detected defects. The main challenge in designing such marker system is to have the markers easily visible and at the same time accurately localizable. This is not trivial because the dark-field detection mechanism is much more sensitive than the other mechanisms. Therefore, a large feature required for visibility in the characterization tool (an SEM or an AFM alignment microscope) will saturate the dark-field detector

of the inspection tool and, thus, impede the spatial accuracy of the latter tool. To solve this problem we developed the stealth marker concept.

2. Methods

2.1 The Rapid Nano

In the Rapid Nano [8], substrates are illuminated with 532 nm laser light under an angle of 60° to the surface normal. The light is TM-polarized to maximize the scattering signal. The scattered light is detected by a charged-coupled device (CCD) camera above the substrate. To increase the signal-to-noise-ratio, the incident light enters intermittently from nine different azimuthal angles. In this way, spurious scattering due to minor local deviations in the blank's surface are reduced. The Rapid Nano can be operated at different laser power levels, ranging from 0.01 to 4.00 W; with higher power smaller particles are visible [10].

2.2 Design and fabrication of the fiducial marker system

A fiducial marker system can be used to increase the re-detection efficacy when samples are transferred from an inspection to a characterization tool. To achieve this, multiple fiducial markers are applied to the blank wafer. The markers should be easily visible and accurately localizable on three platforms: TNO's Rapid Nano, a high-end SEM, and an AFM. Once the markers are found on the Rapid Nano and the characterization tool (SEM or AFM), their positions on both tools are used to construct a linear transformation function that maps the coordinates of the inspection tool to the coordinates of the characterization tool. The transformation function is then used to calculate the positions in the defect map of the Rapid Nano in the coordinates of the characterization tool. Subsequently, the tool operator can navigate directly to these coordinates and quickly re-detect the mapped defects.

Our design of the markers comprises large and small features, so that the markers are at the same time easily visible and accurately localizable in all three tools. A large flat surface provides the visibility and small dots provide the spatial accuracy. The markers are made of a different material than silicon to achieve material contrast in the SEM and color contrast in optical bright field. Their edges scatter strongly in optical dark field. To ensure accuracy in the marker localization under conditions with high inspection sensitivity in the Rapid Nano (i.e., with high laser power), the edge scattering must be minimal. We optimized certain marker parameters to minimize scattering, in particular the composition and the height. The optimization was achieved with experiments and finite element analysis (FEA) modeling. For the latter, we used the Wave Optics module in COMSOL Multiphysics [11].

In our design, 12 fiducial markers are spread across a 100 mm Si blank wafer, see Figure 1a. They are placed in a rectangular grid with a pitch of 20 mm. Each marker consists of either an elongated cross, a T-, or an L-shape with 20 µm wide segments. Furthermore, it has one or two triangles that points to the "north side" of the wafer. Every marker has a unique shape, helping the tool operator to locate all markers once he had found one. Because the markers are applied on top of the silicon substrate, they have raised edges that provide topological contrast. In the center of each marker

small dots are located with a diameter of approximately 150 nm, see the five purple dots in Figure 1b. The central dot is defined as the reference point, or location, of the marker.

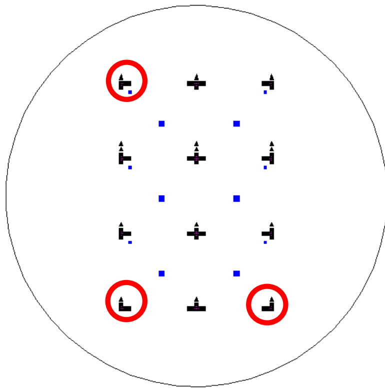

Fig. 1a. Twelve fiducial markers on a 100 mm blank wafer, each with a unique shape. The blue squares show the fields with programmed defects, used for the validation. The encircled markers are used to construct the transformation function in the Monte Carlo simulation and the re-detection experiment.

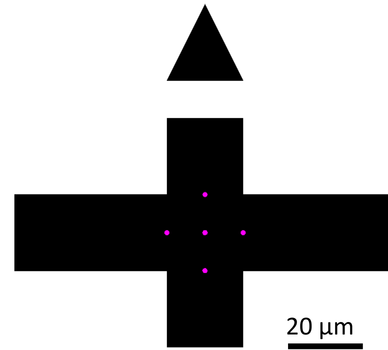

Fig. 1b. An example marker. A marker combines large features (here a cross and a triangle) and small dots, so that the markers are distinguishable, easily visible, and accurately localizable. The 5 central dots are 150 nm in diameter.

The fiducial markers were fabricated on a 100 mm Si wafer with e-beam lithography in a double layer of PMMA. The small central dots were created by overexposing the PMMA, so that the resist tone became negative. After development in MIBK and IPA (1:3), Au or Pt was e-beam evaporated, followed by lift off. The thickness of the deposited film was varied between 20 and 100 nm. No other metals than Au and Pt and no other patterning process than lift off have been investigated.

2.3 COMSOL simulations

COMSOL is a finite element analysis software package that can calculate the physical and materials properties of objects of various composition and shape [11]. We used the *Electromagnetic Waves, Frequency Domain* interface to solve a frequency-domain wave equation for the electric field. Our two-dimensional (2D) domain consists of a Si substrate in vacuum with one fiducial marker, see Fig. 2. The material and the height of the marker are varied. Perfectly matched layers surround the physical domain to absorb all outgoing wave energy, so that no spurious reflections occur at the external boundaries. In the model, the incoming light is defined as an incident field on the upper boundary of the domain. To mimic the conditions in the Rapid Nano, this incoming light is a wide beam with smoothed edges. It has a wavelength of 532 nm, is TM-polarized, and enters under an angle of 60°.

In the Rapid Nano, specularly reflected light travels to a beam dump and only light that scatters into the direction parallel to the substrate normal is detected. Most of the scattering occurs at the edges of the markers. The light that hits the smooth surface in the middle of the marker is reflected and therefore not of interest anymore. To ensure manageable computation time and memory, one marker edge was at the center of the domain and the beam width was kept limited. Contrary to the experiment, the marker was only illuminated from a single azimuth.

The COMSOL interface has an option to solve for the scattered field as a perturbation caused by the fiducial marker to the background field of a homogeneous substrate without the marker. To calculate the background field, the material of the marker is temporary set to vacuum. Figure 2 shows the calculated background field: The light enters from the left and is reflected at the substrate surface. Due to interference between the incoming and the specularly reflected wave, a standing wave pattern appears above the substrate. Approximately 85% - 90% of the incoming light is transmitted into the substrate and absorbed. Next, the material of the marker is changed into a metal and the solution for the background field is used as a basis to calculate the scattered field. The total field is the sum of the background and the scattered field.

The Rapid Nano detects the far electromagnetic field. In COMSOL, the far field is derived from the near field using the Stratton-Chu formula [11]. The amount of scattered light that reaches the detector, is quantified by integrating the far field over the numerical aperture (*NA*) of the Rapid Nano, which is 0.42, see Fig. 2. The integrated far field gives the theoretical amount of detected scattered light due to the fiducial marker in the Rapid Nano. Note that, because of the 2D character of the model, the scattering is expressed in the intensity of scattered light per unit of length.

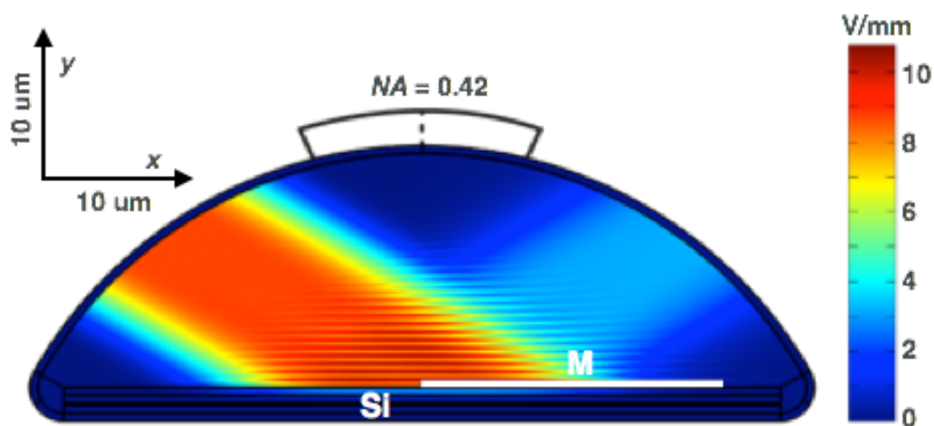

Fig. 2. Example of a 2D COMSOL simulation set-up. The image shows the calculated electric background field, which is the solution of the wave equation without the fiducial marker. It consists of an incoming and a specularly reflected light beam (λ = 532 nm). Interference causes a standing wave pattern above the Si substrate. The white bar indicates the size and position of the marker M (absent in this background simulation); here, the light hits the step up edge of the marker.

2.4 Validation of the fiducial marker system

In order to validate our approach, we determined the re-detection rate of artificial test defects on blank wafers with the fiducial marker system. In particular, we measured the distances between the predicted and the observed positions of the test defects. These distances provide a good estimate for the optimal extent of the search area, such that both the re-detection time and the fraction of missed defects remain within acceptable bounds. To this end, programmed, i.e. artificial, defects were applied to the blank wafer, consisting of ellipses and rectangles of different sizes (from 50 nm to 2 μm) and aspect ratios (1:1, 1:2 and 1:5). They were placed in 12 fields across the wafer, see the blue squares in Fig. 1a.

The test defects were first detected in the Rapid Nano and then re-detected in a scanning electron microscope (FEI Nova NanoSEM 450) and an atomic force microscope (Bruker Dimension FastScan AFM). The locations of three markers (see Fig. 1a) were determined in the stage

coordinates of each tool. Subsequently, linear transformation mappings between the Rapid Nano coordinates and the coordinates of the characterization tools were calculated.

We selected 30 programmed test defects, detected during a Rapid Nano inspection and to be re-detected on the characterization tools. The search areas were chosen sufficiently large (up to 1600 μm^2) to ensure 100% re-detection success with the fiducial marker system. The positions of the defects in the coordinate systems of all tools were recorded.

2.5 Monte Carlo simulations

The re-detection experiment is compared to Monte Carlo simulations, which take into account all uncertainties in the coordinate transformation and the localization of the defects. The accuracy of the transformed coordinates of a defect depends on the uncertainty in the measured marker positions (on the Rapid Nano and the SEM or AFM), the uncertainty in the measured defect position (on the Rapid Nano), and the uncertainty in the transformation function. All these uncertainties are interdependent. Moreover, the final uncertainty in the predicted position of a programmed defect depends on the location on the wafer. In principle, the final uncertainty can be expressed analytically in the basic uncertainties. But in order to simplify the approach and to be more flexible in choosing starting conditions (e.g. the number of markers, their relative positions, the assumed linearity of the transformation function, etc.), we use Monte Carlo simulation to calculate the propagation of uncertainties.

In the Monte Carlo simulation the repeatability in the stage positioning is used as the uncertainty (standard deviation) in the measured position of the markers and defects. The one-dimensional stage repeatability is for the Rapid Nano 1 µm, for the SEM 2 µm, and for the AFM 3 µm. In each Monte Carlo sampling of the simulation, random positions of all markers and programmed defects are chosen, according to Gaussian functions with prescribed centers and widths. Then, the transformation function is derived from the stochastically chosen positions of the three basic markers in the inspection and in the characterization tools. This transformation function is applied to the position of a programmed defect in the inspection tool to get the prediction of the corresponding position in the characterization tool. If all uncertainties in positions were zero, one should find the programmed defect exactly in the center of the SEM or AFM image when one would bring the tool's stage to this predicted position. Actually, the stage in the simulation is brought to the predicted position within the corresponding stage uncertainty. Finally, the distance δ between the chosen stage position and the prescribed defect position is calculated. This procedure is executed for all 30 programmed defects. The sampling procedure is then repeated 100 times and a cumulative distribution function of the distances, though expressed in $\pi\delta^2$, is composed

3. Results and discussion

3.1 Markers on all imaging platforms

To evaluate their performance, the stealth fiducial markers were imaged on all platforms. Indeed, they were easily visible and accurately localizable, see Fig. 3. Because of the material and topographic contrasts, the markers are easily visible in SEM (Fig. 3d), even with a very large field of view (FOV). With a smaller FOV, the small dots become visible (Fig. 3e). An optical microscope is

used to find structures in AFM. The markers are easily visible in optical bright field of the optical microscope of the AFM. Once a marker is found, the cantilever is dropped on its surface. An AFM topography measurement is used to accurately determine the positions of the small central dots.

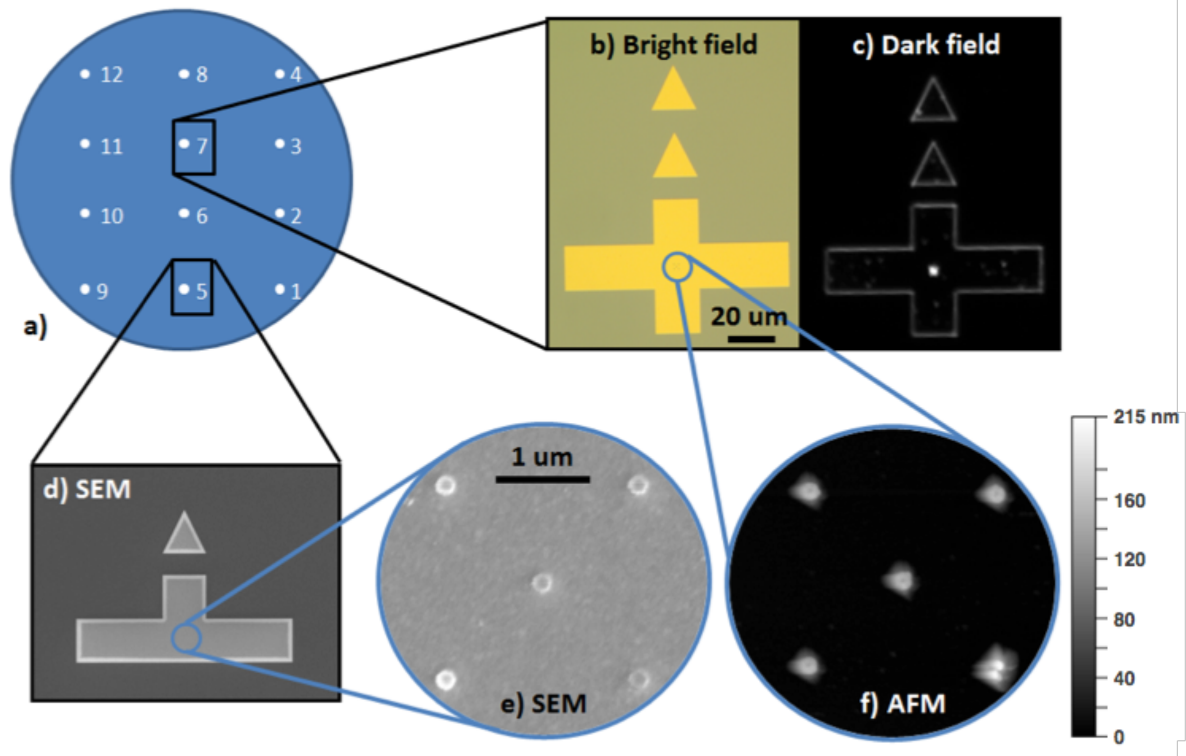

Fig. 3. The stealth fiducial markers on all three platforms. (a) all markers; (b) bright field image of the AFM; (c) Rapid Nano; (d and e) SEM; and (f) AFM. The center of the central dot in (e) and (f) is defined as the location of the marker.

3.2 Optimized stealth fiducial markers

In Fig. 4 the amount of scattering that is detected in the Rapid Nano is plotted versus the height of the marker for a platinum (blue) and a gold (red) marker. From this figure, we conclude that a stealth marker should be made of gold and be as low as possible, preferably 20 nm. We note that a layer thinner than 20 nm will become rough and scatter strongly.

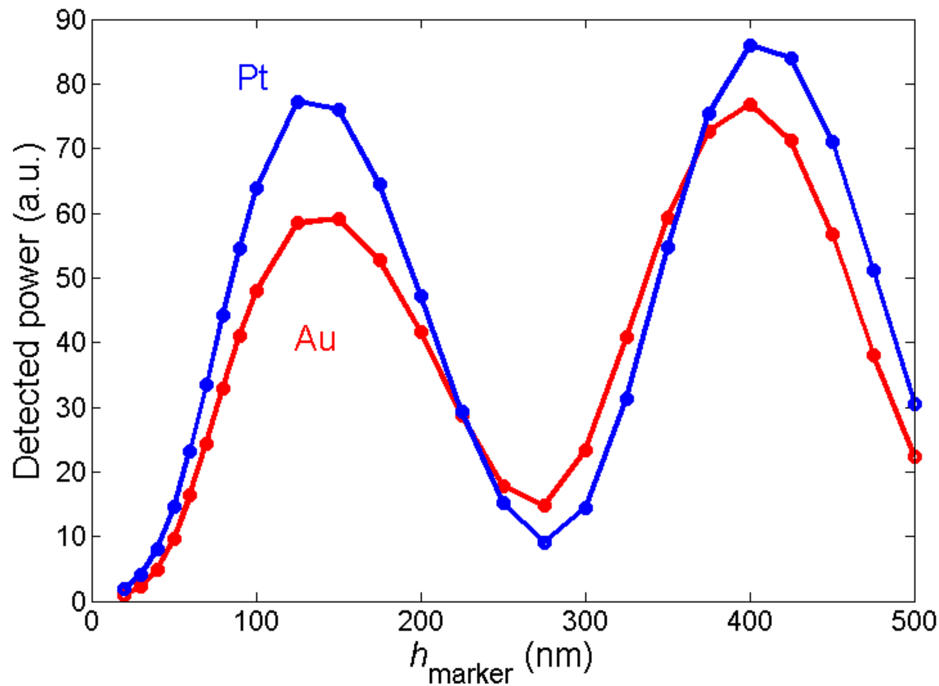

Fig. 4. COMSOL simulation: The amount of scattering in the Rapid Nano versus height, *h*, of Pt and Au markers. A 20 nm Au marker is the best stealth marker. The oscillations in scattered intensities are caused by the standing wave pattern.

This conclusion is confirmed with experiments in the Rapid Nano. We fabricated multiple samples with Pt and Au markers of different heights. Figure 5 shows the scattering of Pt and Au markers of 20 nm. For all powers, the Au marker scatters less that the Pt marker, in line with the COMSOL prediction. Figure 6 shows a comparison of two Au markers, 50 and 20 nm high, respectively. The lower marker scatters appreciably less. In Table 1 the average grey values of the edges in the recorded Rapid Nano images are compared to the integrated far-field intensities of the COMSOL simulations. To ensure the linear range of the detector, only the Rapid Nano images taken at 0.01 W were used. Although no comparison can be made on an absolute scale, the mutual ratios of the experimental results match those of the simulations quite well. The typically 25% variations could be due to roughness of the actual markers edges.

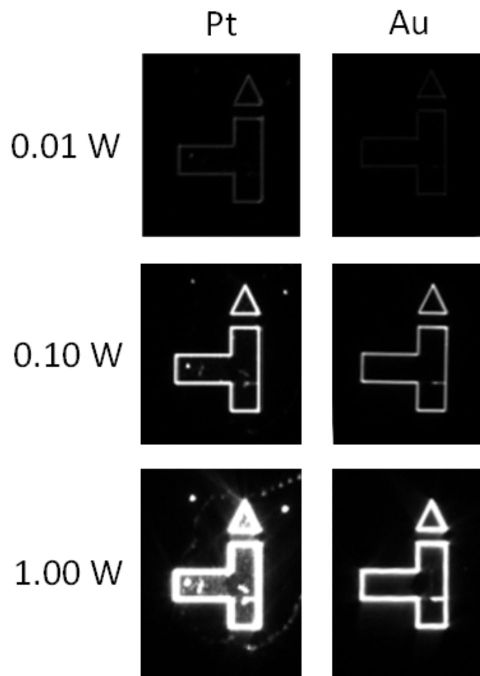

Fig. 5. Dark-field Rapid Nano images of 20 nm high Pt (left) and Au markers (right) for different laser powers. Clearly, the Au marker scatters less.

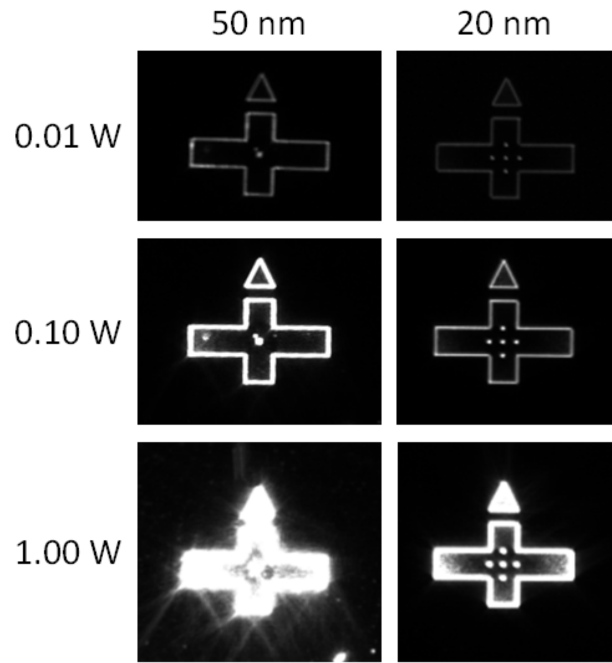

Fig. 6. Dark-field Rapid Nano images of 50 nm (left) and 20 nm (right) high Au markers. The 20 nm markers scatter appreciably less.

Marker	Edge grey value in Rapid Nano image	COMSOL intensity (a.u.)
Pt 20 nm	1567 [5]	1.94
Au 20 nm	588 [5]	0.90
Au 20 nm	684 [6]	0.90
Au 50 nm	4475 [6]	9.61

Table 1. Comparison between measured (at 0.01 W) and calculated edge-scatter intensities. [5]: from Fig. 5; [6]: from Fig. 6.

3.3 Asymmetrical scattering

During the finite element analysis, a peculiar property of the scattering in the Rapid Nano was noticed: Two opposing edges of a fiducial marker scatter differently. The results of the simulations for the step up edge –situation as in Fig. 2– and the step down edge –the opposite edge– of a Au marker are plotted in Fig. 7. Two effects are visible: First, the large oscillations are slightly out of phase with each other. Second, the fist oscillation for the step up edge has lower intensity than that for the step down edge. To our knowledge, this unexpected result has not been reported before for the scattering of TM polarized light, although Otaki has reported asymmetries in the calculated oblique scattering of TE polarized ultra-violet light from EUVL reflection masks [12]. The observed difference in scattering can be explained as follows: TM polarized light enters at 60° to the substrate normal, see Fig. 2. This means that the electric field has *x*- and *y*-components. Light that is reflected from the silicon substrate, gets a 180°-phase shift in the *x*-component. The step up corner of the

marker experiences the sum of two electric fields: One from the direct light and one from the reflected light. Because the marker blocks the nearby substrate, the step down corner receives only direct light. The total electric field at the step up corner has, thus, two opposing contributions in the *x*-direction, while at the step down corner there is only the *x*-component of the direct beam. Therefore, the norm (or amplitude) of the electric field is smaller at the step up corner than at the step down corner. Note that the *y*-component is irrelevant because the Rapid Nano detects light scattered along the surface normal. This asymmetry effect becomes more complicated for higher markers because path length differences come into play as well.

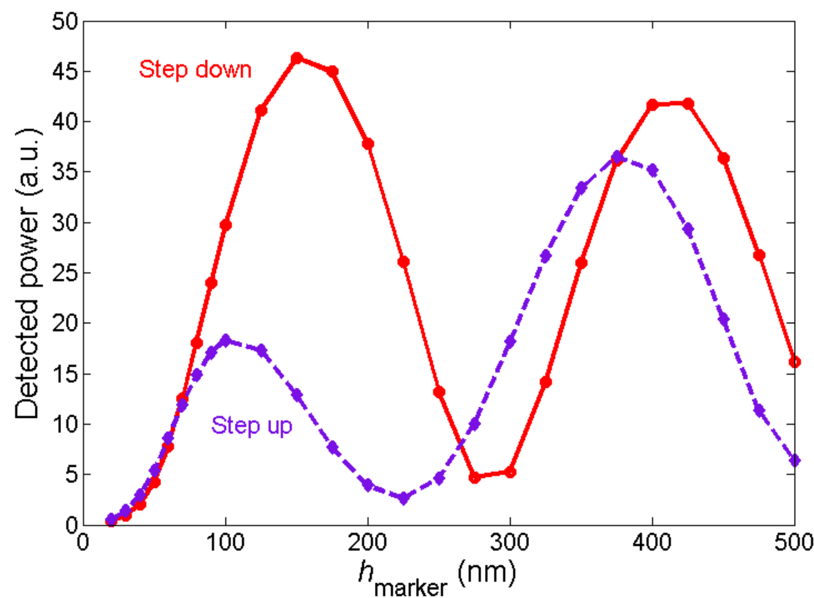

Fig. 7. The step up edge of a fiducial marker produces less scattering than the step down edge.

The asymmetric scattering from the step up and step down edges was also observed experimentally, see Fig. 8. Here, the Rapid Nano illuminated the Au marker from a single azimuthal direction only, as indicated by the white arrows. To ensure a clear effect, the markers were 100 nm high and, to prevent saturation of the Rapid Nano detector, the shutter time was only 4 ms. Figure 8 shows indeed that the step up edge scatters less (average grey value is 2370) than the step down edge (grey value is 3630). This 2:3 ratio corresponds well with the FEA model at 100 nm marker height in Fig. 7.

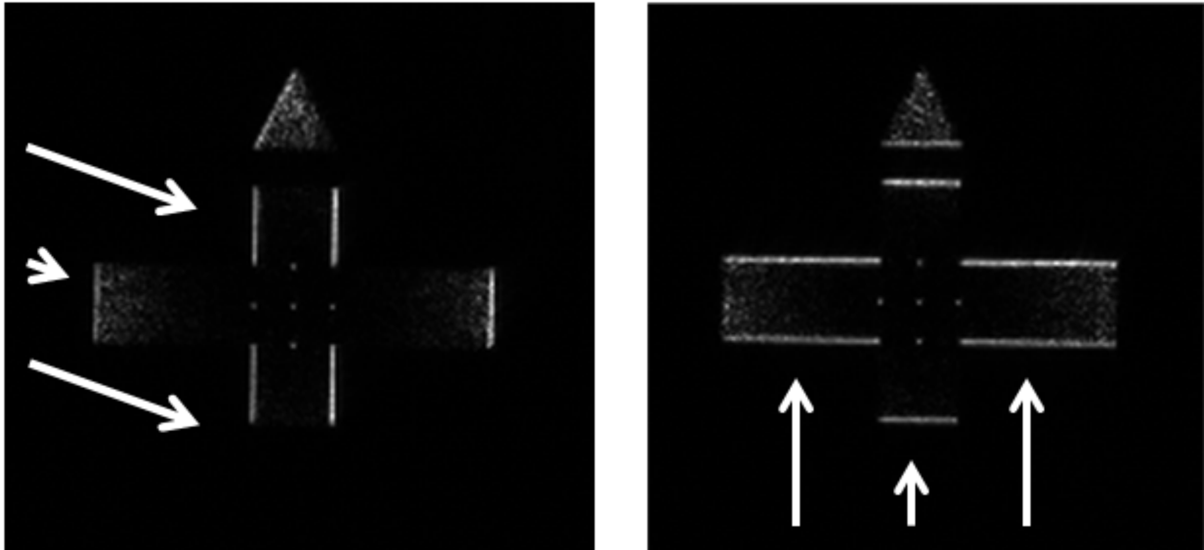

Fig. 8: Experimental observation of the asymmetrical scattering. The Au markers are 100 nm high. The Rapid Nano images were made at 0.01 W, with illumination from a single azimuthal direction, indicated by the white arrows.

3.4 Re-detection rate with the fiducial marker system

As discussed above, the re-detection rate for defects in an SEM without the use of a fiducial marker system is low. If no special precautions are taken, variations in wafer mounting can easily be 0.1 mm or more. If for instance the mounting inaccuracy δ_M in a characterization tool is 60 µm, approximately 50% of the defects would be re-detected in a search area of 2800 µm^2 (=$\pi\delta_M{}^2$) without a fiducial marker system. ITRS requires that the fraction of successful re-detections should be at least 50% [4]. The atomic force microscope is a slower tool than the SEM, which makes the re-detection even more challenging. So far, we had never attempted to re-detect defects on this platform.

The re-detection experiment described above, is used to calculate the hypothetical re-detection rate of defects with a fiducial marker system as a function of the size of the search area. The distances δ between the predicted and the measured positions of all 30 programmed test defects were calculated. In Fig. 9, the calculated set of $\pi\delta^2$'s is plotted along the horizontal axis and the defect number along the vertical axis, ordered according to the magnitude of δ (or $\pi\delta^2$). We call $\pi\delta^2$ the 'search area'. One can see that when the fiducial marker system was used, all 30 defects were found in the SEM within a search area of 200 µm^2. The curves of Fig. 9 can be interpreted as the probability to re-detect a defect as a function of the search area. For instance, if one choses a search area of 50 µm^2, one would have re-detected in the SEM 50% of the (programmed) defects. By comparing the initial parts of the re-detection probability curves, we see that with an SEM the fiducial marker system (blue full curve) improves the re-detection rate with a factor of 55 (purple dashed curve). This number is obviously only a rough estimate, based on the assumed wafer mounting inaccuracy of 60 µm. We note that there exist no reliable records for the re-detection of defects on blank wafers without a fiducial marker system.

The ITRS requirement of 50% re-detection is met if an area of 50 µm^2 around the predicted location is imaged in the SEM, thus e.g. a single 7×7 µm^2 image will do. The minimal amount of pixels a defect needs to comprise in order to be visible, depends on the contrast and noise in the SEM

image. As a rule of thumb ten pixels suffice. A standard SEM image is typically 1000 pixels wide, so particles down to 70 nm would be re-detectable. Therefore only one standard SEM image per particle is needed to comply with the ITRS requirement on re-detection probability for particles down to 70 nm. For the smallest particles the Rapid Nano can detect, with a diameter of 42 nm, effectively 3 standard SEM images are sufficient.

The re-detection efficacy for the AFM is lower than for the SEM. This is, however, not an intrinsic weakness of the AFM but related to the specific apparatus used in this study, lacking a proper backlash correction of the stage positioning. The stage accuracy could be improved by approaching each mapped defect always from, e.g., the positive *x*- and *y*-directions.

The experimental results are compared to the predicted uncertainties in the position of the defects, calculated with the Monte Carlo simulations, see the dashed curves in Fig. 9. The average distance $<\delta>$ between the predicted and measured positions of the mapped defects is 3.7 μm for the SEM and 9.4 μm for the AFM. Whereas the average predicted distances in the simulations are 4.0 μm and 6.0 μm, respectively. The results of the SEM match nicely, but the AFM performs worse because of the backlash in the stage.

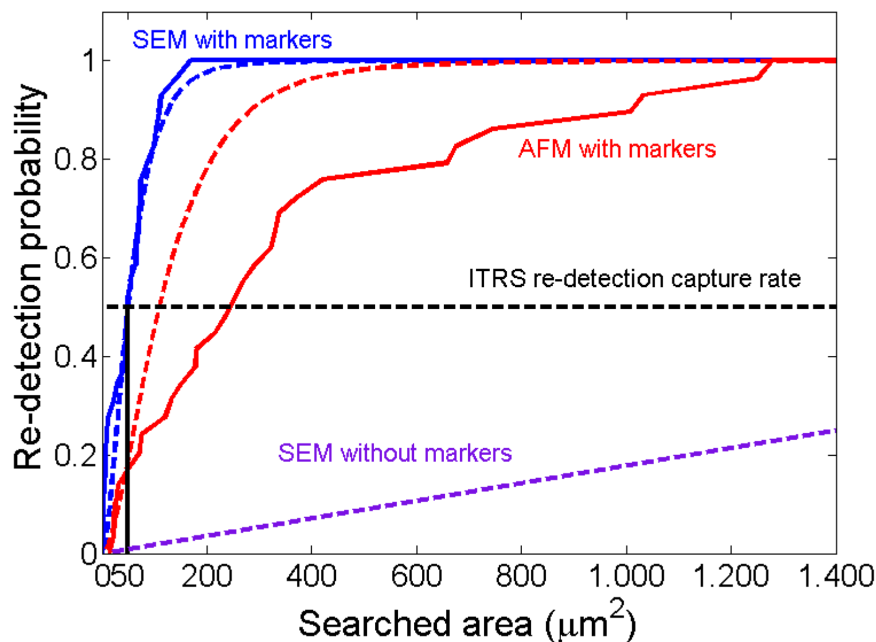

Fig. 9. Experimental and simulation results for programmed defects, re-detected in SEM (blue full curve) and AFM (red full curve). The black dashed line indicates the ITRS requirement and the purple dashed line is an estimate for the re-detection rate on an SEM without a fiducial marker system. Only one standard 7x7 μm^2 SEM image per defect particle is needed to comply with the ITRS requirement. The re-detection efficacy for AFM is less because of an incidental lower stage positioning accuracy. The blue dashed curve is a Monte Carlo simulation for the SEM, agreeing well with the experiment. There is no agreement between the AFM simulation (red dashed) and the AFM experiment (red full) because of the poorer AFM stage positioning accuracy.

4. Conclusions

Experiments and COMSOL simulations showed that large (20-100 μm) but thin (20 nm) Au fiducial markers with (150 nm) small features, are very visible in optical bright field and in SEM, while almost invisible (stealth) in optical dark field. These properties make the markers both easily visible and

accurately localizable in the characterization (or review) tools. The validation experiments showed that the developed fiducial marker system greatly enhances the re-detection rate of defects. Without a fiducial marker system a re-detection rate of 50% was considered challenging, but in the experiments with the fiducial marker system 100% of 30 programmed defects were re-detected on both a scanning electron microscope and an atomic force microscope. In fact, only one standard SEM (7x7 μm^2) image per particle is needed with the fiducial marker system to comply with the ITRS requirement of 50% re-detection probability for particles down to 70 nm. For the smallest particles the Rapid Nano can detect, 42 nm in diameter, 3 standard SEM images are needed.

The experimental SEM results are in agreement with the results of Monte Carlo simulations for the uncertainties in the prediction of the positions of the defects. The AFM performed worse than expected; the likely cause is stage backlash. A peculiar property of the scattering in the Rapid Nano was noticed: Two opposing edges of a fiducial marker scatter differently. This asymmetry was observed both in COMSOL simulations as in experiment.

The developed fiducial marker system will be used to redetect and characterize defects found with the Rapid Nano. Further optimization is needed, e.g. by using Al that is more compatible with semiconductor manufacturing and etching that yield less surface contamination. The characterization and classification of defects in review tools such as SEM or AFM will aid in locating and eliminating the source of the particle defects in semiconductor manufacturing equipment.

References

[1] Gordon E. Moore, Proc. IEEE 86 (1998) 82–85.

[2] E. Karl, Z. Guo, J.W. Conary, J.L. Miller, Y.-G. Ng, S. Nalam, D. Kim, J. Keane, U. Bhattacharya, K. Zhang, Dig. Techn. Papers - IEEE Intern. Solid-State Circuits Conf. 58 (2015) 310-311.

[3] R. Kirsch, U. Zeiske, Proc. SPIE 7971 (2011) 79712M.

[4] International Technology Roadmap for Semiconductors 2013 (ITRS). http://www.itrs.net/.

[5] J.K. Stortelder, J.C.J. van der Donck, S. Oostrom, P. van der Walle, O. Brux, P. Dress, Proc. SPIE 7969 (2011) 79691Q.

[6] Hideo Ota, Masayuki Hachiya, Yoji Ichiyasu, Toru Kurenuma, Hitachi Rev. 55 (2006) 78-82.

[7] Ardavan Zandiatashbar, Byong Kim, Young-kook Yoo, Keibock Lee, Ahjin Jo, Ju Suk Lee, Sang-Joon Cho, Sang-il Park, Proc. SPIE 9424 (2015) 94241X.

[8] Peter van der Walle, Sandro Hannemann, Daan van Eijk, Wouter Mulckhuyse, Jacques C.J. van der Donck, Proc. SPIE 9050 (2014) 905033.

[9] Hamed Sadeghian, Bert Dekker, Rodolf Herfst, Jasper Winters, Alexander Eigenraam, Ramon Rijnbeek, Nicole Nulkes, Proc. SPIE 9424 (2015) 94240O.

[10] Peter Van der Walle, Pragati Kumar, Dmitry Ityaksov, Richard Versluis, Diederik J. Maas, Jochem Janssen, Jacques C.J. Van Der Donck, Proc. SPIE 8681 (2013) 868116.

[11] COMSOL v5.0 Wave Optics Module User's Guide, 2014. http://www.comsol.com/ .

[12] K. Otaki, Jpn. J. Appl. Phys. 39 (2000) 6819-6826.

Acknowledgements

This work was performed in the framework of the E450LMDAP project. TNO gratefully acknowledges funding by the ECSEL Joint Undertaking and the Netherlands Enterprise Agency (RVO). We thank Anja van Langen-Suurling, Gaurav Nanda, Ruud Schmits, and Hans van den Berg for assistance with the sample preparations and Maarten van Es for the AFM work.